Journal of Computational Physics 228 (2009) 7497–7512

Contents lists available at ScienceDirect

Journal of Computational Physics

journal homepage: www.elsevier.com/locate/jcp

Unconditionally convergent nonlinear solver for hyperbolic conservation laws with S-shaped flux functions

Patrick Jenny [a,*], Hamdi A. Tchelepi [b], Seong H. Lee [c]

[a] Institute of Fluid Dynamics, ETH Zurich, Sonneggstrasse 3, CH-8092 Zurich, Switzerland
[b] Dept. of Energy Resources Engineering, Stanford University, USA
[c] Chevron Company, 6001 Bollinger Canyon Rd., San Ramon, 94583-2324 CA, USA

ARTICLE INFO

Article history:
Received 5 January 2009
Received in revised form 25 May 2009
Accepted 10 June 2009
Available online 3 July 2009

Keywords:
Implicit discretization
Non-convex flux
Conservation laws
Nonlinear analysis
Upwinding
Multiphase flow

ABSTRACT

This paper addresses the convergence properties of implicit numerical solution algorithms for nonlinear hyperbolic transport problems. It is shown that the Newton–Raphson (NR) method converges for any time step size, if the flux function is convex, concave, or linear, which is, in general, the case for CFD problems. In some problems, e.g., multiphase flow in porous media, the nonlinear flux function is S-shaped (not uniformly convex or concave); as a result, a standard NR iteration can diverge for large time steps, even if an implicit discretization scheme is used to solve the nonlinear system of equations. In practice, when such convergence difficulties are encountered, the current time step is cut, previous iterations are discarded, a smaller time step size is tried, and the NR process is repeated. The criteria for time step cutting and selection are usually based on heuristics that limit the allowable change in the solution over a time step and/or NR iteration. Here, we propose a simple modification to the NR iteration scheme for conservation laws with S-shaped flux functions that converges for any time step size. The new scheme allows one to choose the time step size based on accuracy consideration only without worrying about the convergence behavior of the nonlinear solver. The proposed method can be implemented in an existing simulator, e.g., for CO_2 sequestration or reservoir flow modeling, quite easily. The numerical analysis is confirmed with simulation studies using various test cases of nonlinear multiphase transport in porous media. The analysis and numerical experiments demonstrate that the modified scheme allows for the use of arbitrarily large time steps for this class of problems.

1. Introduction

A wide range of CFD problems, including multiphase flow dynamics in porous media, are described by nonlinear hyperbolic conservation laws. Various methods are used to solve these conservation equations numerically [7]. Explicit time integration schemes offer accuracy and computational efficiency as long as the limit on the stable time step size is not a major concern [5]. In some problems, however, the time step restriction associated with an explicit scheme is quite severe, and the use of implicit schemes is necessary. In reservoir simulation problems [1], where the evolution of the saturation field in the geologic porous formation, as a function of space in time is sought, it is often the case that for a given global time step size, the CFL numbers in the computational domain can vary by orders of magnitude [6]. In such cases, the use of explicit time integration schemes is simply not feasible, and implicit time integration is required [1,3].

* Corresponding author. Tel.: +41 44 632 6987.
E-mail address: jenny@ifd.mavt.ethz.ch (P. Jenny).

0021-9991/$ - see front matter © 2009 Elsevier Inc. All rights reserved.
doi:10.1016/j.jcp.2009.06.032

One approach for dealing with problems where the CFL numbers vary widely across the computational domain is the use of adaptive implicit/explicit schemes. In these adaptive strategies, an unknown in the computational domain is treated either explicitly, or implicitly, for a given time increment [10,4]; heuristics [10], or linear stability analysis [2] can be used to label a particular unknown as explicit or implicit. However, even if an adaptive (mixed-implicit) approach is used, there is no guarantee that the nonlinear solver, which is usually based on the Newton method, will converge for the unknowns that are treated implicitly.

In the Newton method, a sequence of iterates, each involving the construction (Jacobian matrix computation) and solution of the resulting linear system, is performed until the solution of the nonlinear algebraic equations is obtained for the target time step [8]. The solution from the previous time step is usually used as the starting point for the Newton iterations. Once a converged solution is obtained, one proceeds with the next time step. This approach is straightforward, and for conservation laws where the flux function is convex (shock), concave (rarefaction wave), or linear (contact discontinuity), the Newton scheme is unconditionally stable. However, for S-shaped flux functions, like for most problems involving nonlinear multiphase flow and transport in porous media, the Newton method does not converge for time steps that are too large [1]. In reservoir simulation, this problem is usually overcome by empirical time step control techniques. The use of such heuristics often leads to time step sizes that are too conservative resulting in unacceptably large computational time and wasted computations.

Here, we present convergence maps and a theoretical convergence analysis of implicit solution algorithms for transport problems governed by first-order hyperbolic conservation laws with S-shaped flux functions, and we propose a simple modification of the Newton method that results in an unconditionally convergent iterative scheme. We point out that truncation errors, due to the use of large time steps, are not the focus of this paper. Instead, our objective is to deal with problems where the convergence behavior of the nonlinear solver is the controlling factor in selecting the time steps in the course of a simulation. Since issues related to the convergence of the nonlinear solver are resolved by using the scheme proposed here, the time step size for modeling this class of large-scale nonlinear problems can be chosen solely based on accuracy (time truncation error) considerations.

In Section 2, the model problem and a standard solution algorithm are introduced. In Section 3, the convergence behavior of implicit solution algorithms for hyperbolic problems is investigated. In Section 4, we present a simple modification that leads to unconditional convergence, and we demonstrate the modified scheme using challenging two-phase flow problems. The conclusions are given in Section 5.

2. Model problem and standard solution algorithm

We consider the hyperbolic equation

$$\frac{\partial S}{\partial t} + \nabla \cdot (f(S)\boldsymbol{u}) = 0 \quad \text{on} \quad \Omega. \tag{1}$$

Eq. (1) describes the convection of the dependent variable S ($0 \leqslant S \leqslant 1$), where f is the nonlinear flux function of S with $0 \leqslant f \leqslant 1$, and $\boldsymbol{u}$ is a given velocity field, which can have significant spatial variability in the domain at a given time. For simplicity, but without loss of generality, $\boldsymbol{u}$ is considered constant in time, and we assume that $f' = df/dS \geqslant 0$. The nonlinear transport problem can be solved iteratively using the Newton–Raphson method as outlined in the flow diagram of Fig. 1 leading to the solution S^{n+1} at the new time level. In each iteration step $\nu + 1$, the linearized transport equation is solved (represented by the operator T), which results in an updated saturation field $S^{n+1,\nu+1}$. When the maximum absolute change in the saturation between iterations anywhere in the domain is less than an appropriately defined threshold, ε, the nonlinear loop is considered converged and $S^{n+1,\nu+1}$ is taken as the solution S^{n+1} at the new time level.

Next, we study a 3D discretization of Eq. (1), which is based on implicit Euler time integration and first-order upwinding [1,7]. For simplicity, an orthogonal, uniformly spaced grid of which each cell (control-volume) can be identified by an index triplet $I = (i,j,k)$ is considered. This leads to the nonlinear scheme

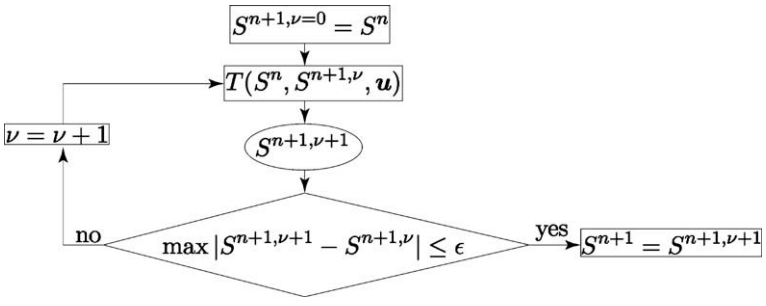

Fig. 1. Flow diagram of one time step using the Newton–Raphson method; solving the linearized transport equation is represented by the operator T.

$$\frac{S_I^{n+1}-S_I^n}{\tau}+\sum_{m=1}^{3}\left\{\frac{[f^{n+1}u_m]_{I_m^+}-[f^{n+1}u_m]_{I_m^-}}{h_m}\right\}=0. \tag{2}$$

The superscripts n and $n+1$ denote the old and new time levels, respectively, τ is the time step size, h_1, h_2 and h_3 are the grid spacings in the three coordinate directions. The index triplets $I_m^{\pm}=I\pm\delta I_m/2$ denote quantities at the faces of cell I, where $\delta I_1=(1,0,0), \delta I_2=(0,1,0)$ and $\delta I_3=(0,0,1)$. Note that for simple upwinding

$$[fu_m]_{I_m^-}=F\left(f_{I-\delta I_m},f_I,[u_m]_{I_m^-}\right) \quad \text{and} \quad [fu_m]_{I_m^+}=F\left(f_I,f_{I+\delta I_m},[u_m]_{I_m^+}\right), \tag{3}$$

with

$$F(a,b,c)=\begin{cases} ac & \text{if} \quad c>0,\\ bc & \text{else.}\end{cases} \tag{4}$$

In order to solve the nonlinear algebraic system (2), the flux $f^{n+1}=f(S^{n+1})$ is approximated by the linearization

$$f^{n+1}\approx f^{n+1,\nu+1}=f^{n+1,\nu}+\underbrace{\left(\frac{df}{dS}\right)^{n+1,\nu}}_{f'^{n+1,\nu}}\left(S^{n+1,\nu+1}-S^{n+1,\nu}\right), \tag{5}$$

where the superscript $n+1,\nu+1$ denotes the iteration level $\nu+1$ during the time step $n+1$. Then, a new approximation $S^{n+1,\nu+1}$ of S^{n+1} is computed by solving the linearized system

$$\left[\frac{S^{n+1,\nu+1}-S^n}{\tau}+\frac{f^{n+1,\nu}+f'^{n+1,\nu}(S^{n+1,\nu+1}-S^{n+1,\nu})}{\alpha}\right]_I=\beta_I^{n+1,\nu+1}, \tag{6}$$

with

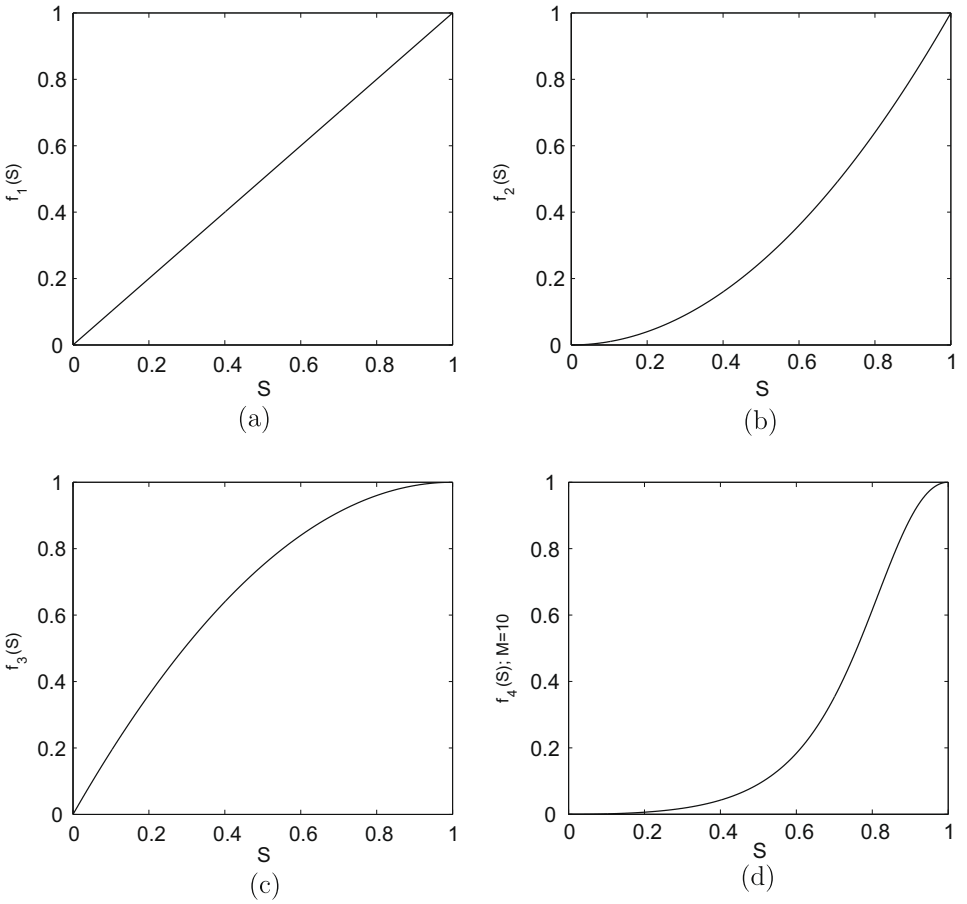

Fig. 2. Linear (a), convex (b), concave (c) and S-shaped (d) functions $f_1(S)$, $f_2(S)$, $f_3(S)$ and $f_4(S)$ (with $M=10$), respectively, which are used for the convergence analysis in this paper.

$$\frac{1}{\alpha_I} = \sum_{m=1}^{3} \left\{ \frac{H([u_m]_{I_m^+})[u_m]_{I_m^+} - H([-u_m]_{I_m^-})[u_m]_{I_m^-}}{h_m} \right\}, \tag{7}$$

and

$$\beta_I^{n+1,\nu+1} = \sum_{m=1}^{3} \left\{ \frac{H([u_m]_{I_m^-})[f^{n+1,\nu} + f'^{n+1,\nu}(S^{n+1,\nu+1} - S^{n+1,\nu})]_{I-\delta I_m}[u_m]_{I_m^-}}{h_m} \right\} - \sum_{m=1}^{3} \left\{ \frac{H([-u_m]_{I_m^+})[f^{n+1,\nu} + f'^{n+1,\nu}(S^{n+1,\nu+1} - S^{n+1,\nu})]_{I+\delta I_m}[u_m]_{I_m^+}}{h_m} \right\}, \tag{8}$$

which is obtained by substituting the right-hand side of Eq. (5) for f^{n+1} in Eq. (2); $H(\cdot)$ denotes the Heaviside function. We note that it is important to enforce the constraint $0 \leqslant S^{n+1,\nu+1} \leqslant 1$, which is justified by the physics, after every iteration. Rearranging the previous expressions leads to the simple form

$$\left[\underbrace{f^{n+1,\nu} + \frac{\alpha}{\tau} S^{n+1,\nu}}_{g(S^{n+1,\nu})} + \underbrace{\left(f'^{n+1,\nu} + \frac{\alpha}{\tau}\right)}_{g'(S^{n+1,\nu})} (S^{n+1,\nu+1} - S^{n+1,\nu}) = \gamma^{n+1,\nu+1} \right]_I, \tag{9}$$

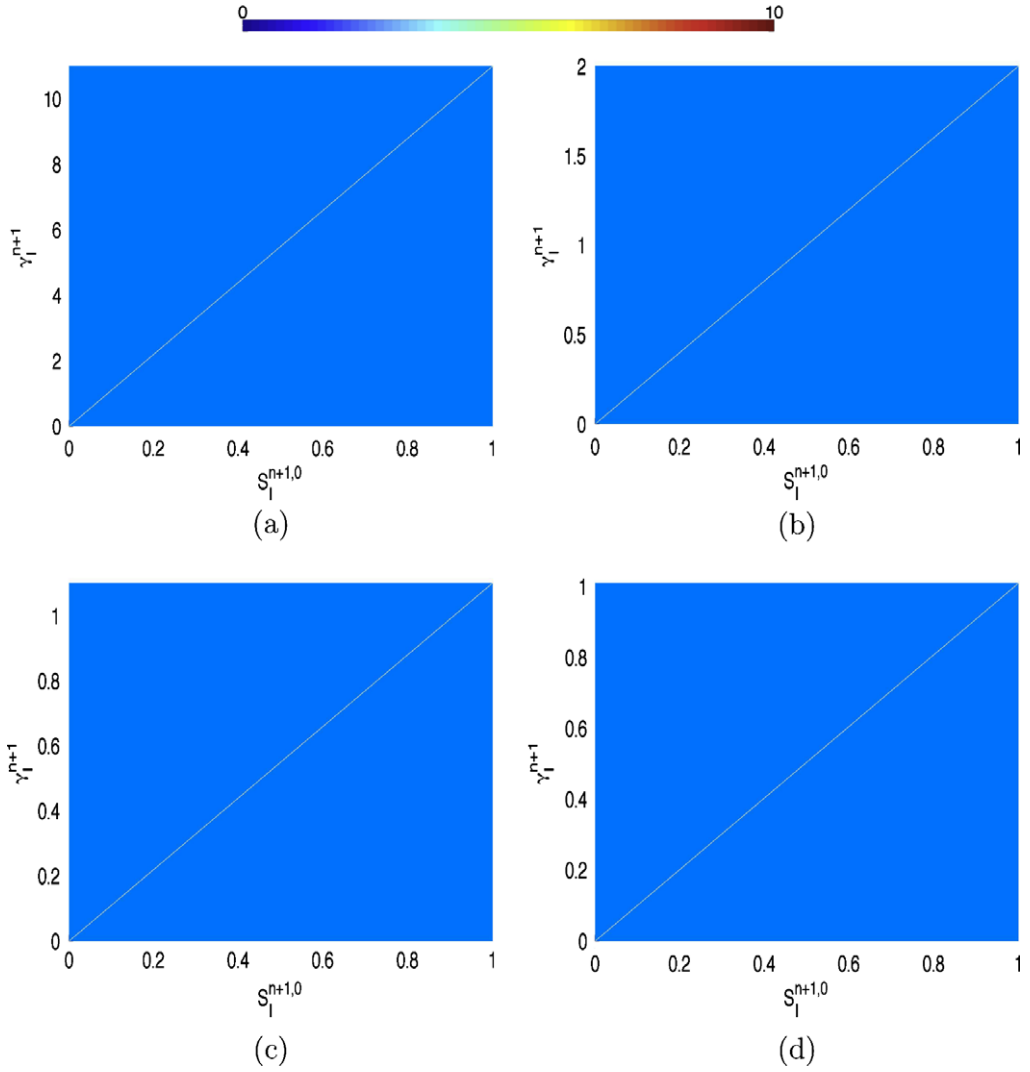

Fig. 3. Standard Newton–Raphson scheme: convergence maps for the linear function $f(S) = f_1(S), \alpha_I \equiv 1$, and $\tau = 0.1$ (a), $\tau = 1$ (b), $\tau = 10$ (c) and $\tau = 100$ (d). The colors in the S_I^n–γ_I^{n+1}-plane refer to the convergence rate of the scheme (11); dark blue means fast (1 iteration) and dark red slow (10 iterations) convergence; white indicates no convergence. As expected, only one iteration is required for all τ. (For interpretation of the references to colour in this figure legend, the reader is referred to the web version of this article.)

where

$$\gamma^{n+1,v+1} = \alpha\left(\beta^{n+1,v+1} + \frac{S^n}{\tau}\right). \tag{10}$$

To study the nonlinear convergence behavior, we now assume that $\gamma_I^{n+1} = \gamma_I^{n+1,v+1}$ is known and fixed for all iteration levels v. Eq. (9) can be rearranged as

$$S_I^{n+1,v+1} = \max\left(0, \min\left(1, S_I^{n+1,v} + \frac{\gamma_I^{n+1} - g(S_I^{n+1,v})}{g'(S_I^{n+1,v})}\right)\right), \tag{11}$$

for the new value $S_I^{n+1,v+1}$ with the function $g(S) = f(S) + S\alpha/\tau$. The function g as well as γ_I^{n+1} depend on the time step size, which must be chosen such that

$$0 \leqslant \gamma_I^{n+1} \leqslant g(1), \tag{12}$$

is satisfied. Note that since for proper boundary conditions, the assumption that γ_I^{n+1} is already known always applies for at least one grid cell I, where convergence has not been achieved yet. This can be demonstrated by using a potential-based (flow direction) ordering of the equation and unknowns [6]. Thus, the isolated study of the iteration scheme (11) for a given control-volume allows us to make general conclusions about the convergence behavior of scheme (7).

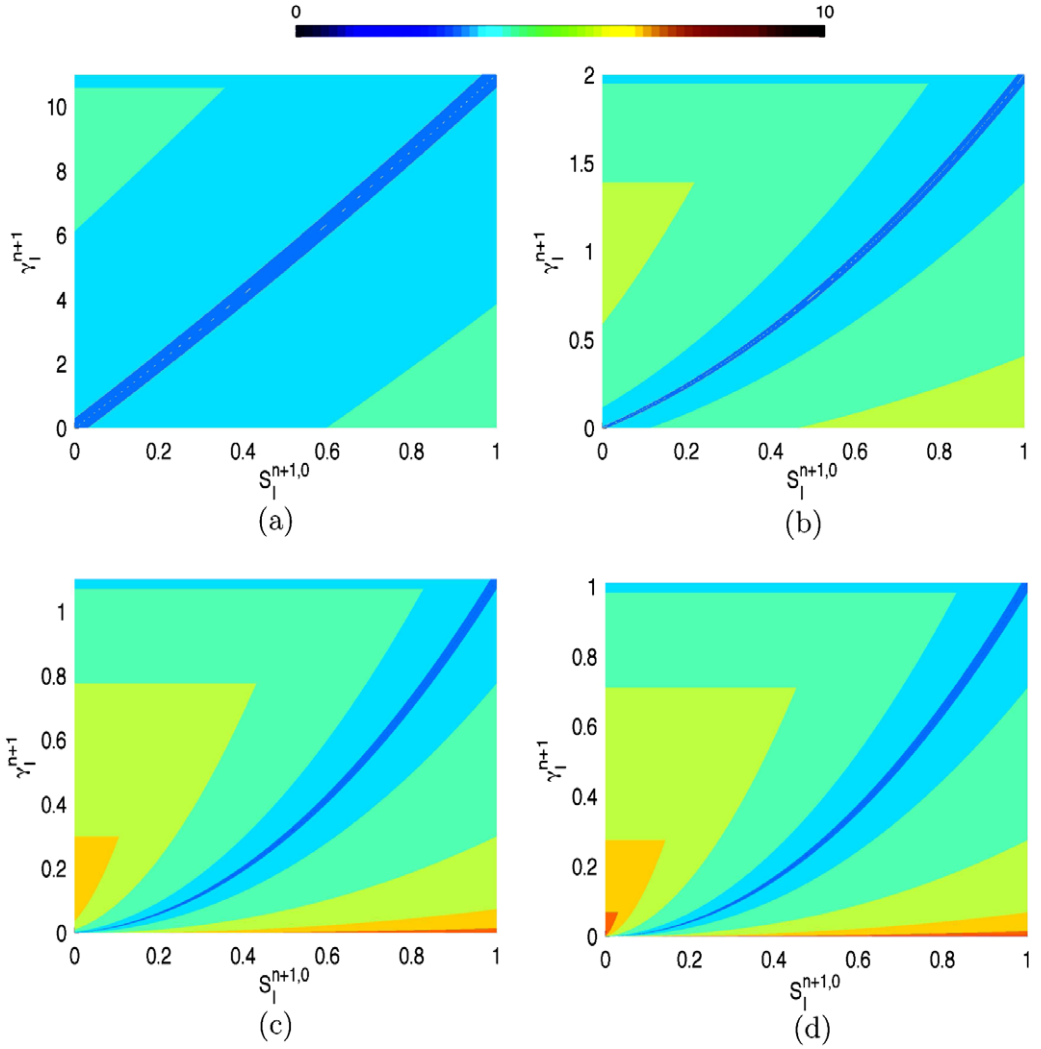

Fig. 4. Standard Newton–Raphson scheme: convergence maps for the convex function $f(S) = f_2(S)$, $\alpha_I \equiv 1$, and $\tau = 0.1$ (a), $\tau = 1$ (b), $\tau = 10$ (c) and $\tau = 100$ (d). The colors in the S_I^n–γ_I^{n+1}-plane refer to the convergence rate of the scheme (11); dark blue means fast (1 iteration) and dark red slow (10 iterations) convergence; white indicates no convergence. As expected, no white regions exist, which indicates that the scheme is unconditionally convergent for any τ. (For interpretation of the references to colour in this figure legend, the reader is referred to the web version of this article.)

3. Convergence analysis

Here, we investigate the stability and convergence rate of scheme (11) for different combinations of $f(S), S_I^{n+1,0} = S_I^n, \gamma_I^{n+1}, \alpha_I$ and τ.

For a more rigorous theoretical understanding, the following theorem is introduced:

Theorem 1. *The iteration scheme*

$$S^{\nu+1} = h(S^\nu) = \max\left(0, \min\left(1, S^\nu + \frac{g(S^\infty) - g(S^\nu)}{g'(S^\nu)}\right)\right), \tag{13}$$

with $0 \leqslant S_1 \leqslant S^\infty \leqslant S_2 \leqslant 1$ *is considered, where the function* $g(S) \in C^2$ *fulfills*

$$((\forall S \in [S_1, S_2] : g'(S) \geqslant 0) \vee (\forall S \in [S_1, S_2] : g'(S) \leqslant 0)) \wedge \ ((\forall S \in [S_1, S_2] : g''(S) \geqslant 0) \vee ((\forall S \in [S_1, S_2] : g''(S) \leqslant 0)). \tag{14}$$

In this case, it follows that

$$\forall S^\nu \in \{S : S_1 \leqslant S \leqslant S_2 \wedge |g'(S)| > |g'(S^\infty)|\} : |S^\infty - h(S^\nu)| \leqslant |S^\infty - S^\nu| \wedge (S^\infty - h(S^\nu))(S^\infty - S^\nu) \geqslant 0. \tag{15}$$

Proof. $\forall S^\nu \in \{S : S_1 \leqslant S \leqslant S_2 \wedge |g'(S)| > |g'(S^\infty)|\}$ one can write

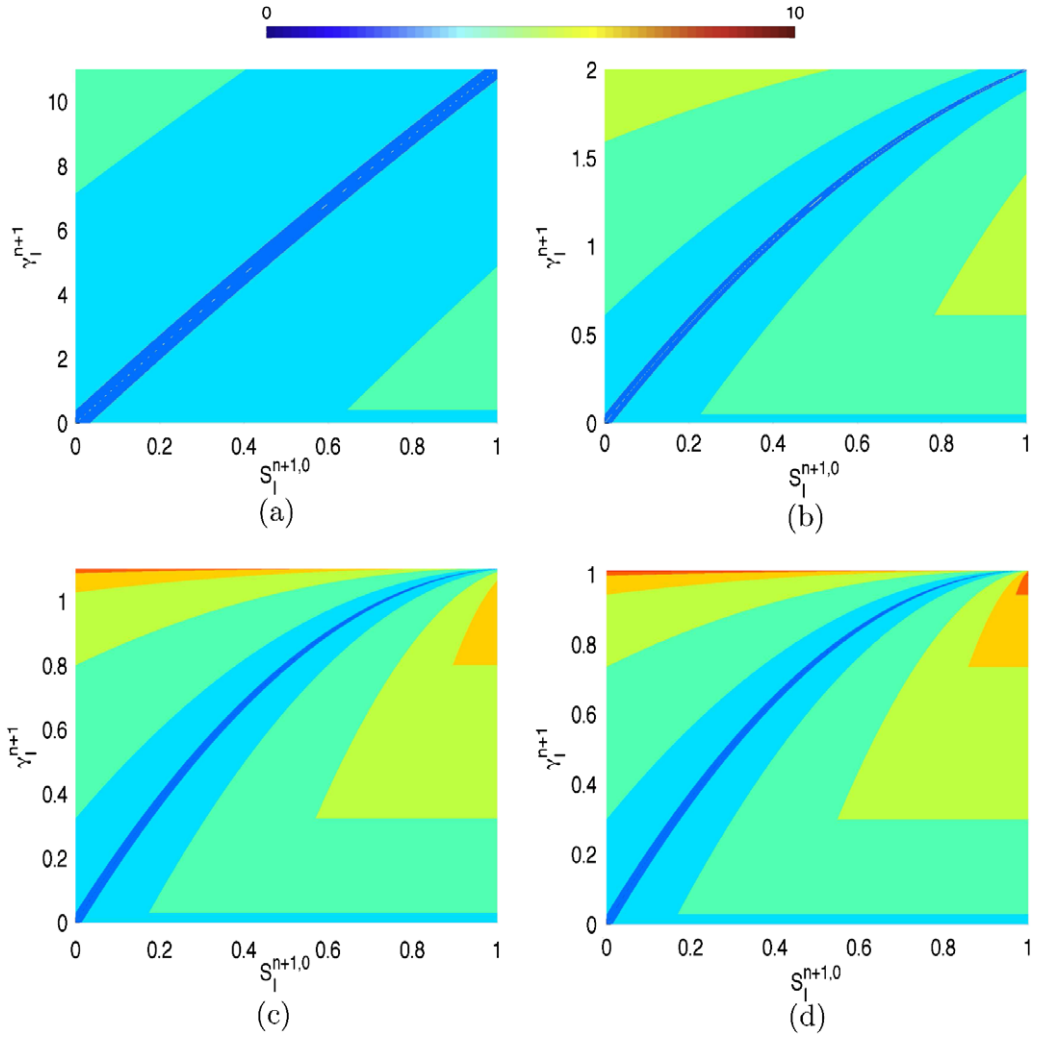

Fig. 5. Standard Newton–Raphson scheme: convergence maps for the concave function $f(S) = f_3(S), \alpha_I \equiv 1$, and $\tau = 0.1$ (a), $\tau = 1$ (b), $\tau = 10$ (c) and $\tau = 100$ (d). The colors in the S_I^n–γ_I^{n+1}-plane refer to the convergence rate of the scheme (11); dark blue means fast (1 iteration) and dark red slow (10 iterations) convergence; white indicates no convergence. As expected, no white regions exist, which indicates that the scheme is unconditionally convergent for any τ. (For interpretation of the references to colour in this figure legend, the reader is referred to the web version of this article.)

$$g(S^\infty) = g(S^v) + \eta(S^\infty - S^v), \tag{16}$$

with $0 \leqslant \eta/g'(S^v) \leqslant 1$. Comparison with

$$g(S^\infty) = g(S^v) + g'(S^v)(S^* - S^v), \tag{17}$$

leads to

$$S^* - S^v = \frac{g(S^\infty) - g(S^v)}{g'(S^v)} = \frac{\eta}{g'(S^v)}(S^\infty - S^v), \tag{18}$$

$$\Rightarrow 0 \leqslant \frac{S^* - S^v}{S^\infty - S^v} = \frac{\eta}{g'(S^v)} \leqslant 1, \tag{19}$$

$$\Rightarrow 0 \leqslant \frac{(S^\infty - S^v) - (S^\infty - S^*)}{S^\infty - S^v} \leqslant 1, \tag{20}$$

$$\Rightarrow 0 \leqslant 1 - \frac{S^\infty - S^*}{S^\infty - S^v} \leqslant 1, \tag{21}$$

$$\Rightarrow 0 \leqslant \frac{S^\infty - S^*}{S^\infty - S^v} \leqslant 1. \tag{22}$$

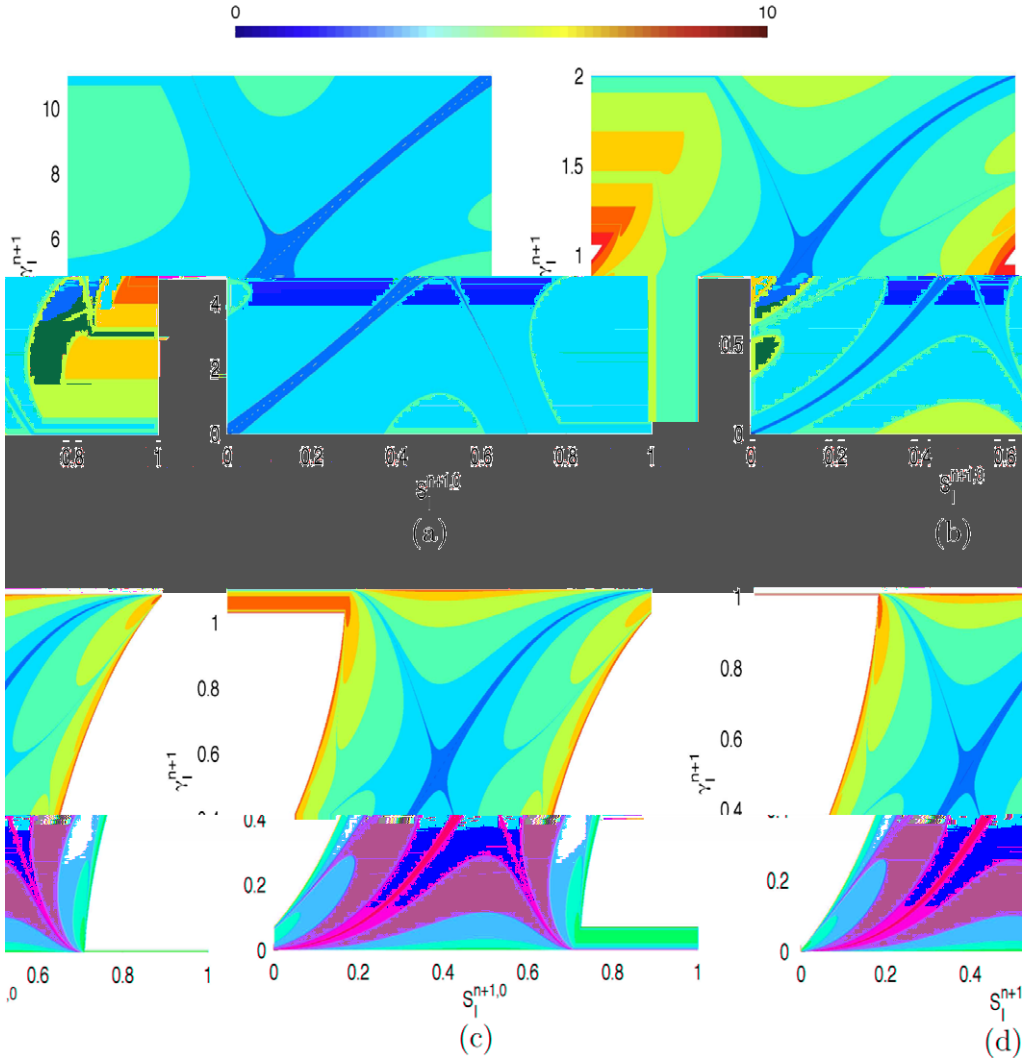

Fig. 6. Standard Newton–Raphson scheme: convergence maps for the S-shaped function $f(S) = f_4(S)$ with $M = 1$, $\alpha_l \equiv 1$, and $\tau = 0.1$ (a), $\tau = 1$ (b), $\tau = 10$ (c) and $\tau = 100$ (d). The colors in the S_l^n–γ_l^{n+1}-plane refer to the convergence rate of the scheme (11); dark blue means fast (1 iteration) and dark red slow (10 iterations) convergence; white indicates no convergence. (For interpretation of the references to colour in this figure legend, the reader is referred to the web version of this article.)

From Eq. (22) follows that

$$|S^\infty - S^*| \leqslant |S^\infty - S^\nu| \quad \text{and that} \quad (S^\infty - S^*)(S^\infty - S^\nu) \geqslant 0, \tag{23}$$

which leads to either

$$0 \leqslant S^\infty \leqslant S^* \leqslant S^\nu \leqslant 1 \quad \text{or} \quad 0 \leqslant S^\nu \leqslant S^* \leqslant S^\infty \leqslant 1, \tag{24}$$

and together with Eqs. (13) and (17) one can write

$$S^* = h(S^\nu). \tag{25}$$

Finally, from (24) and (25), we get

$$\forall S^\nu \in \{S : S_1 \leqslant S \leqslant S_2 \wedge |g'(S)| > |g'(S^\infty)|\} : |S^\infty - h(S^\nu)| \leqslant |S^\infty - S^\nu| \wedge (S^\infty - h(S^\nu))(S^\infty - S^\nu) \geqslant 0. \quad \square \tag{26}$$

Theorem 1 states that $S^{\nu+1} = h(S^\nu)$ and S^ν are on the same side of S^∞, and that $S^{\nu+1}$ is closer to S^∞ than S^ν, if there exists a range containing both S^ν and S^∞, in which the monotonous function $g(S)$ is convex, concave, or linear, and if $|g'(S^\nu)| \geqslant |g'(S^\infty)|$. Note that with the substitutions $S_I^{n+1,\nu} = S^\nu$ and $\gamma_I^{n+1} = g(S^\infty)$ the iteration schemes (11) and (13) are equivalent.

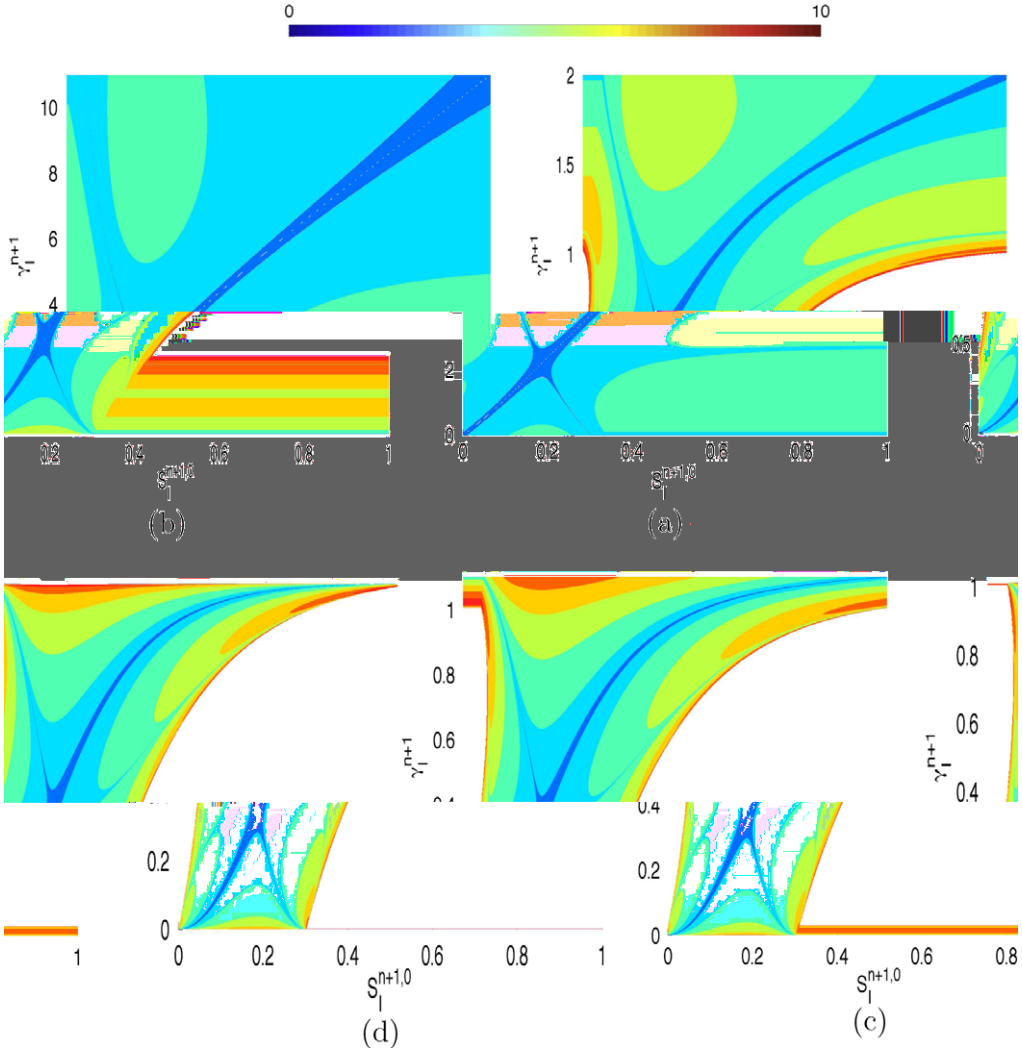

Fig. 7. Standard Newton–Raphson scheme: convergence maps for the S-shaped function $f(S) = f_4(S)$ with $M = 0.1$, $\alpha_I \equiv 1$, and $\tau = 0.1$ (a), $\tau = 1$ (b), $\tau = 10$ (c) and $\tau = 100$ (d). The colors in the S_I^n–γ_I^{n+1}-plane refer to the convergence rate of the scheme (11); dark blue means fast (1 iteration) and dark red slow (10 iterations) convergence; white indicates no convergence. (For interpretation of the references to colour in this figure legend, the reader is referred to the web version of this article.)

Now we consider the following functions for $f(S)$:

$$f_1(S) = S, f_2(S) = S^2, f_3(S) = 1 - (1-S)^2 \quad \text{and} \quad f_4(S) = \frac{S^2}{S^2 + M(1-S)^2}, \tag{27}$$

which are linear, convex, concave, and S-shaped, respectively (see Fig. 2). For all functions, studies with $\tau \in \{0.1, 1, 10, 100\}$ and $\alpha_I \equiv 1$ are performed. In addition, for $f(S) = f_4(S)$, all possible combinations with $M \in \{0.1, 1, 10\}$ are investigated. This results in 24 cases, for which we study the behavior of the Newton–Raphson scheme. In each case, we determine for all points $(S_I^{n+1,0}, \gamma_I^{n+1}) \in [0,1] \times [0, g(1)]$, if the solution $S_I^{n+1} = g^{-1}(\gamma^{n+1})$ is found by scheme (11) as $v \to \infty$, i.e., if

$$\lim_{v\to\infty} g(S_I^{n+1,v}) = \gamma_I^{n+1}. \tag{28}$$

The colors in Figs. 3–5, 7 and 8 depict the number of iterations required until the convergence criterion $|S_I^{n+1,v+1} - S_I^{n+1,v}| \leqslant \epsilon = 10^{-4}$ is satisfied. Specifically, dark blue means fast (one iteration) and dark red means slow (10 iterations) convergence; the white regions in the S_I^n-γ_I^{n+1}-phase space indicate that no convergence is achieved after 20 iterations.

From the convergence maps shown in Figs. 3–5, one can observe that scheme (11) is unconditionally convergent for linear, convex, and concave functions $f(S)$. That is, for any $\gamma_I^{n+1} \in [0, g(1)]$, the solution $S_I^{n+1} = g^{-1}(\gamma_I^{n+1})$ is found from any initial guess $S_I^{n+1,0} = S_I^n \in [0,1]$ independent of the time step size $\tau \in \{0.1, 1, 10, 100\}$.

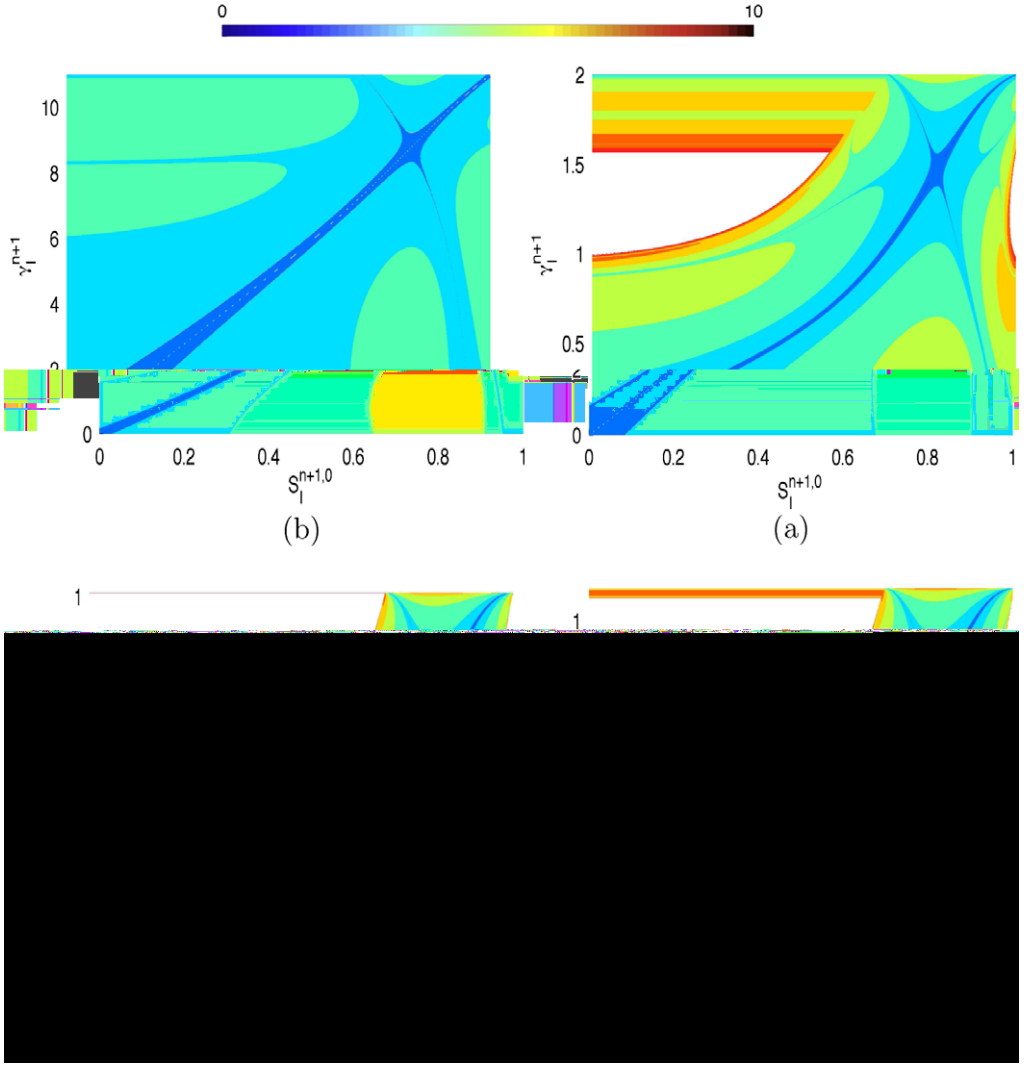

Fig. 8. Standard Newton–Raphson scheme: convergence maps for the S-shaped function $f(S) = f_4(S)$ with $M = 10$, $\alpha_I \equiv 1$, and $\tau = 0.1$ (a), $\tau = 1$ (b), $\tau = 10$ (c) and $\tau = 100$ (d). The colors in the S_I^n–γ_I^{n+1}-plane refer to the convergence rate of the scheme (11); dark blue means fast (1 iteration) and dark red slow (10 iterations) convergence; white indicates no convergence. (For interpretation of the references to colour in this figure legend, the reader is referred to the web version of this article.)

This is consistent with Theorem 1. We have $0 = S_1 \leqslant S_I^{n+1,0} \leqslant S_2 = 1$ with $g'(S) > 0$ for all $S \in [S_1, S_2]$ and either $\forall S \in [S_1, S_2] : g''(S) \geqslant 0$ or $\forall S \in [S_1, S_2] : g''(S) \leqslant 0$, i.e., the conditions for Theorem 1 are fulfilled. For $S_I^{n+1,0}$ with $|g'(S_I^{n+1,0})| \geqslant |g'(S^\infty)|$, Theorem 1 guarantees that all $S_I^{n+1,v>0}$ are on the same side of $S^\infty = g^{-1}(\gamma_I^{n+1})$ and that $\lim_{v\to\infty} S_I^{n+1,v} = S^\infty$. On the other hand, if $\neg(|g'(S_I^{n+1,0})| \geqslant |g'(S^\infty)|), S_I^{n+1,0}$ and $S_I^{n+1,1}$ are on opposite sides of S^∞, but all $S_I^{n+1,v>0}$ are on the same side and approach S^∞ as $v \to \infty$.

For S-shaped functions $f(S)$, the situation is different. Figs. 6–8 show the convergence maps for $f(S) = f_4(S)$ with $M = 1, M = 0.1$ and $M = 10$, respectively. For very small time steps ($\tau = 0.1$), scheme (11) is convergent, i.e., the phase plane contains no white regions. However, the fraction of white area in the considered domain increases rapidly for larger time steps ($\tau \in \{1, 10, 100\}$).

While the implicit convection scheme (7) is unconditionally stable for linear, convex, and concave flux functions, the above analysis of the iteration Eq. (11) reveals that small time steps are required to achieve stability, if the flux function has an S-shape (concave–convex).

While these findings are consistent with the numerical experiences in reservoir simulation practice, the non-convexity of the flux function has not been clearly identified as a major cause of nonlinear convergence problems. Moreover, a detailed convergence analysis of the nonlinear iteration scheme has not been performed. To our knowledge, the only exception is the work of Peaceman [9], where he performed a nonlinear stability analysis of the hyperbolic conservation equations for two-phase transport in porous media with the usual S-shaped flux function. He concluded that the stability limit of the implicit scheme did not depend on the local throughput (CFL) condition, but on the amount of allowable change in the solution (saturation) over a time step. Peaceman pointed out the difficulty of determining the 'allowable change amount' a priori. Moreover, he pointed to stability difficulties associated with large changes in the solution variable during a time step (usually an indication of a large time step), when the second derivative of the flux function was not uniformly negative. However, his results were not conclusive, and they did not lead to an improved nonlinear solution strategy of the discretized conservation laws.

3.1. 2D test case

To demonstrate the convergence problem of the convection scheme (7) with S-shaped flux functions, a rectangular domain $\Omega = [0, 120] \times [0, 60]$ with a uniform 120×60 grid is considered. First, a divergence-free velocity field $\boldsymbol{u} = -\lambda \nabla \boldsymbol{p}$ was computed by solving the elliptic equation

$$\nabla \cdot (\lambda \nabla p) = -q \quad \text{on} \quad \Omega, \tag{29}$$

for p with the boundary condition

$$\nabla p \cdot \boldsymbol{n} = 0 \quad \text{at} \quad \partial\Omega, \tag{30}$$

and source and sink terms $q = 1$ and $q = -1$ in the sub-domains $\Omega_{in} = [0, 1] \times [0, 1]$ and $\Omega_{out} = [119, 120] \times [59, 60]$, respectively ($\boldsymbol{n}$ is the unit normal vector at the boundary $\partial\Omega$ pointing outward). The spatially varying coefficient, λ, is defined for each grid cell; its base-10 logarithm is shown in Fig. 9. The resulting velocity, $\boldsymbol{u}$, is then employed to approximately solve Eq. (1) using scheme (7). In the following studies, we refer to the normalized time $t^* = tq/7200$. Initially, $S \equiv 0.1$ in the whole domain, and for $t^* > 0, S \equiv 1$ in Ω_{in}. Fig. 10 shows the distribution of S after one time step for $f(S) = f_4(S)$ with $M = 1$ and $\tau = 0.005$ (top), $f(S) = f_2(S)$ with $\tau = 0.005$ (middle), and $f(S) = f_2(S)$ with $\tau = 0.5$ (bottom).

Strong oscillations occur with $f(S) = f_4(S)$, although the time step size $\tau = 0.005$ is relatively small. The same scheme is stable with $f(S) = f_2(S)$ for the same time step size; moreover, the same scheme is stable even for a time step that is 100

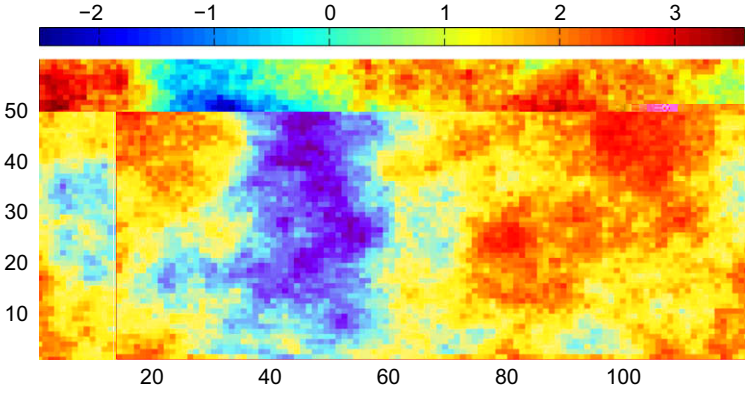

Fig. 9. Domain of 2D test case: shown is the base-10 logarithm of λ; blue means low and red means high values. (For interpretation of the references to colour in this figure legend, the reader is referred to the web version of this article.)

times larger (the number of iterations was limited to 200). Next, the origin of the instability (convergence problem) is investigated for the local scheme (11). Then, based on these findings, a simple modification resulting in an unconditionally convergent nonlinear iteration scheme is devised.

4. Unconditionally convergent solution algorithm

The convergence maps in Figs. 3–5, 7 and 8 show that the iteration Eq. (11) converges for all possible target values γ_l^{n+1}, if $S_l^{n+1,0} = S^c$, where S^c is the inflection point of the function $f(S)$ with $f''|_{S^c} = d^2f/dS^2|_{S^c} = 0$ (note that curvature and inflection point are the same for both $f(S)$ and $g(S)$).

This is predicted by Theorem 1. There exist two possibilities: one with $S_1 = S^c \leqslant S^\infty = g^{-1}(\gamma_l^{n+1}) \leqslant S_2 = 1$ and one with $S_1 = 0 \leqslant S^\infty \leqslant S_2 = S^c$. In both cases, $S^c \in [S_1, S_2]$ and $0 \leqslant g'(S^\infty) \leqslant g'(S^c)$, and therefore Theorem 1 ensures for $S_l^{n+1,v} = S^c$ that all $S_l^{n+1,\mu \geqslant v}$ are on the same side of S^∞ and that $\forall \mu \geqslant v : |S_l^{n+1,\mu+1} - S^\infty| \leqslant |S_l^{n+1,\mu} - S^\infty|$; i.e. with the Newton–Raphson scheme, one obtains $\lim_{\mu\to\infty} S_l^{n+1,\mu>v} = S^\infty$, if one starts the Newton–Raphson iterations with $S_l^{n+1,v} = S^c$.

4.1. First modified scheme

This finding suggests setting $S_l^{n+1,v+1} = S^c$ at the end of each Newton–Raphson iteration $v+1$, if the curvature f'' has opposite signs at $S_l^{n+1,v}$ and $S_l^{n+1,v+1}$. The resulting nonlinear solver is unconditionally convergent even for S-shaped flux functions.

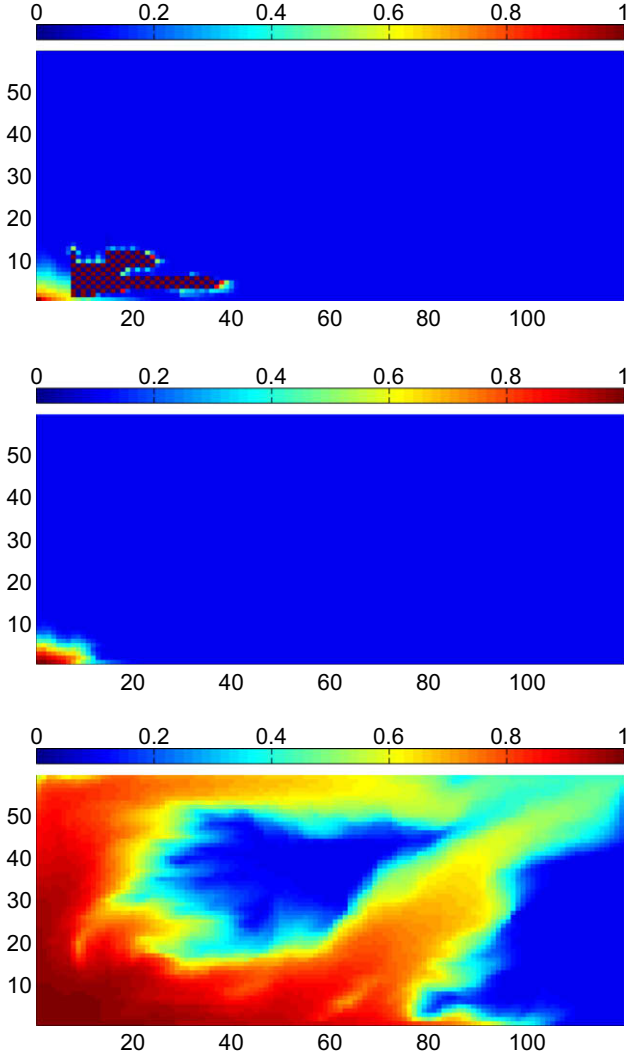

Fig. 10. Distribution of S after one time step: with $f(S) = f_4(S)$ ($M = 1$) after $t^* = 0.005$ and $\tau = 0.005$ (top), with $f(S) = f_2(S)$ after $t^* = 0.005$ and $\tau = 0.005$ (middle), with $f(S) = f_2(S)$ after $t^* = 0.5$ and $\tau = 0.5$ (bottom).

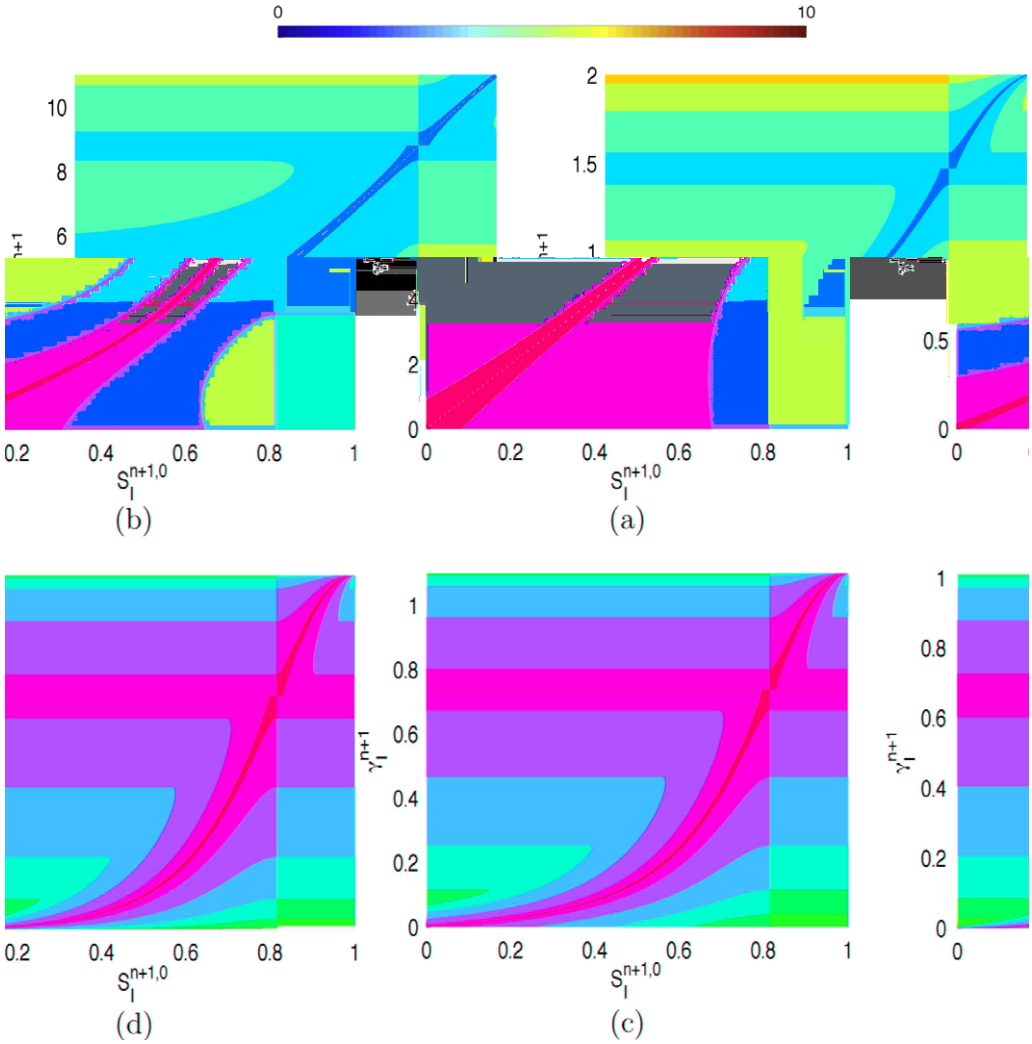

Fig. 11. First modified scheme: convergence maps for the S-shaped function $f(S) = f_4(S)$ with $M = 10, \alpha_l \equiv 1$, and $\tau = 0.1$ (a), $\tau = 1$ (b), $\tau = 10$ (c) and $\tau = 100$ (d). The colors in the S_l^n–γ_l^{n+1}-plane refer to the convergence rate of the scheme (11); dark blue means fast (1 iteration) and dark red slow (10 iterations) convergence; white indicates no convergence. No white regions exist indicating that the scheme is unconditionally convergent for any τ. (For interpretation of the references to colour in this figure legend, the reader is referred to the web version of this article.)

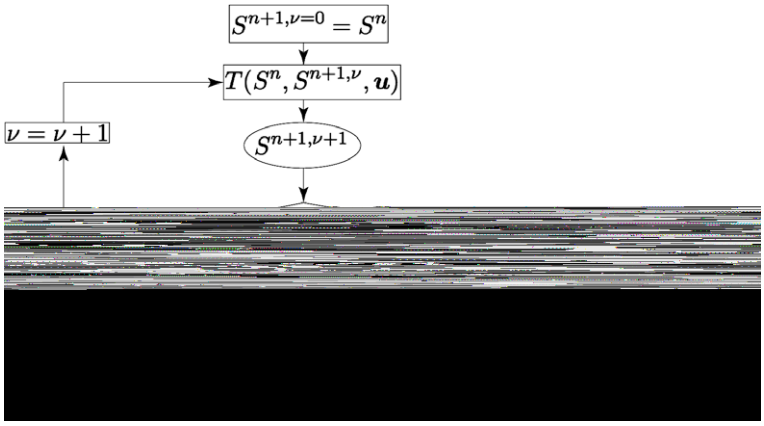

Fig. 12. Flow diagram of one time step using the second modified scheme; solving the linearized transport equation is represented by the operator T.

This is referred to as the first modified scheme. Convergence (stability) for large and small time steps is confirmed by the convergence maps of the first modified scheme with $f(S) = f_4(S), M = 10, \alpha \equiv 1$ and $\tau \in \{0.1, 1, 10, 100\}$ shown in Fig. 11, which contain no white regions.

4.2. Second modified scheme

The first modification of the iterative convection scheme (7) described above is straightforward. In some practical cases, however, it may be difficult, or costly, to determine the exact location of the inflection point. Therefore, a second modified scheme that is easier to implement in a general setting is proposed. This scheme differs from the first modified scheme only in the way $S_I^{n+1,\nu+1}$ is modified at the end of each Newton–Raphson iteration. Instead of setting $S_I^{n+1,\nu+1}$ to S^c, selective under-relaxation is applied, i.e., $S_I^{n+1,\nu+1}$ is replaced by $(S_I^{n+1,\nu+1} + S_I^{n+1,\nu})/2$, if the signs of f'' at $S_I^{n+1,\nu}$ and $S_I^{n+1,\nu+1}$ are not the same; otherwise, $S_I^{n+1,\nu+1}$ remains unchanged. A diagram of the second modified scheme is shown in Fig. 12. Since it is straightforward to determine the curvatures of f, the alternative, second modification can easily be implemented in an existing simulator. Fig. 13 depicts convergence maps for the second modified scheme with $f(S) = f_4(S), M = 10, \alpha \equiv 1$ and $\tau \in \{0.1, 1, 10, 100\}$. Similar to the convergence maps of the first modified scheme, no white regions exist, which confirms that the second modified scheme is convergent, even for extremely large time steps. For comparison, convergence maps of the Newton–Raphson scheme with under-relaxation (unconditional with a relax-

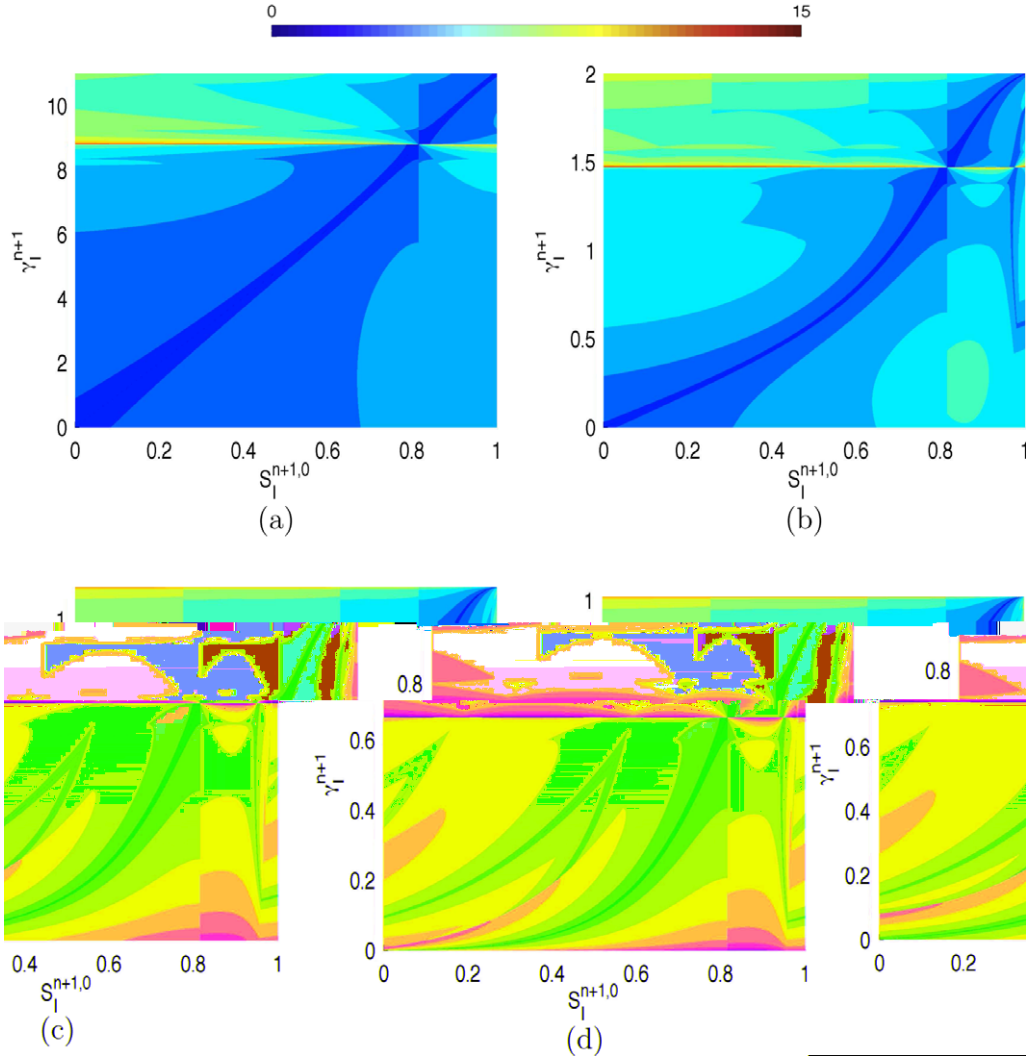

Fig. 13. Second modified scheme: convergence maps for the S-shaped function $f(S) = f_4(S)$ with $M = 10, \alpha_I \equiv 1$, and $\tau = 0.1$ (a), $\tau = 1$ (b), $\tau = 10$ (c) and $\tau = 100$ (d). The colors in the S_I^n–γ_I^{n+1}-plane refer to the convergence rate of scheme (11); dark blue means fast (1 iteration) and dark red slow (15 iterations) convergence; white indicates no convergence. No white regions exist indicating that the scheme is unconditionally convergent for any τ. (For interpretation of the references to colour in this figure legend, the reader is referred to the web version of this article.)

ation factor of 0.5) with $f(S) = f_4(S), M = 10, \alpha \equiv 1$ and $\tau \in \{0.1, 1, 10, 100\}$ are shown in Fig. 14. The dominance of red in the plots of Fig. 14 indicates that typically many iterations are required to reach convergence, which is in contrast to the dominance of dark blue in the plots of Fig. 13 indicating that, on average, only few iterations are required with the second modified scheme.

4.3. Numerical experiments

In this section, we demonstrate that both modified schemes work quite well when used with the convection scheme (7) as predicted by the analysis of the iteration Eq. (11). It is also shown that the two modified schemes are almost equally efficient. Moreover, for very small time steps, the efficiency is the same as that of the unmodified Newton–Raphson scheme. On the other hand, efficiency is significantly compromised, if convergence is achieved by unconditional under-relaxation after each iteration.

For the following studies, the test case described in Section 3.1 is employed with $f(S) = f_4(S), M = 1$ and different values for τ. All the simulations were performed with both modified schemes, and we demonstrate that arbinst oftv60Td[(1)-37l-

modified schemes are convergent for all τ. Note that while the saturation field appears more dispersed in the lower plots of Fig. 15 due to large time truncation errors, the solution is consistent with the discrete representation of physics and is free of oscillations. Therefore, the new nonlinear solution method allows for choosing the time step size solely based on accuracy considerations (i.e., space and time truncation errors) without worrying about the stability (convergence behavior) of the nonlinear solver.

In all cases, the number of required iterations is similar for the two modified schemes. This is illustrated in Fig. 16, where convergence histories of one large time step ($\tau = 0.5$) are shown for the two modified schemes and for Newton–Raphson with consequent (unconditional) under-relaxation with a relaxation factor of 0.5. Note that Newton–Raphson with under-relaxation is also stable, but requires significantly more iterations to converge.

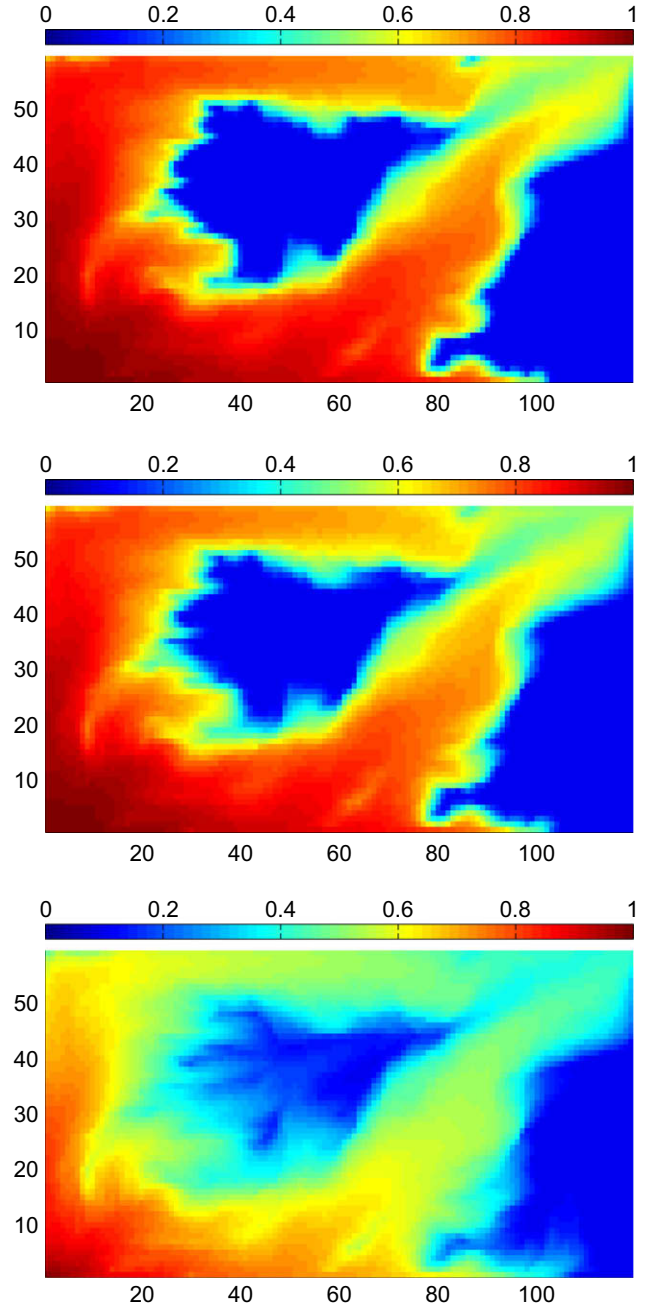

Fig. 15. Scalar S after $t^* = 0.5$ for $f(S) = f_4(S)$ ($M = 1$) using the second modified scheme: with $\tau = 0.005$ (top), with $\tau = 0.05$ (middle) and with $\tau = 0.5$ (bottom).

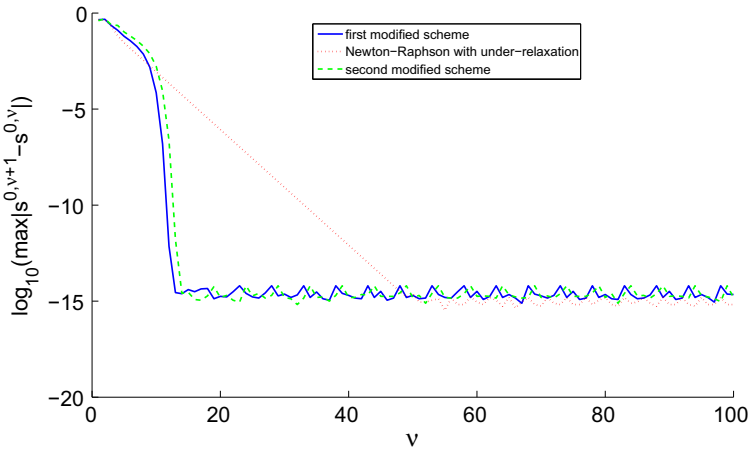

Fig. 16. Convergence histories of on time step of size $\tau = 0.5$ for $f(S) = f_4(S)$ $(M = 1)$ with the first modified scheme, the second modified scheme, and Newton–Raphson with under-relaxation.

5. Conclusions

We analyzed the convergence problems associated with the Newton–Raphson scheme for solving the algebraic systems associated with implicit discretization of nonlinear transport equations with S-shaped flux functions, which are of interest in modeling multi-phase flow and transport in porous media, for example. The convergence problems of standard Newton methods are tied to the properties of the flux function in the conservation law and dependence on the initial guess and the size of the desired time step. Based on a detailed analysis, we proposed an unconditionally convergent iterative solution algorithm that employs a simple modification of the classical Newton–Raphson iteration scheme and requires minimal effort to be implemented in an existing simulator. Theoretical analysis indicates that the modified scheme is unconditionally convergent for any time step size, and this was demonstrated using challenging numerical problems of two-phase flow, where we spanned a very wide range of the parameter space of interest. The convergence rate and computational efficiency of the proposed schemes are expected to improve both the robustness and overall efficiency of large-scale simulation problems significantly. The new unconditionally convergent iteration schemes allow one to choose the time step size solely based on accuracy considerations related to the physics being modeled (e.g., time truncation error) as opposed to being limited by convergence difficulties associated with the nonlinear solver itself.

References

[1] K. Aziz, A. Settari, Petroleum Reservoir Simulation, Elsevier, London, 1979.
[2] K.H. Coats, Impes stability: selection of stable timesteps, Soc. Petrol. Eng. J. 8 (2) (2003) 181–187.
[3] K.H. Coats, L.K. Thomas, R.G. Pierson, Compositional and black oil reservoir simulation, SPE Res. Eval. Eng. (1998) 372–379.
[4] P.A. Forsyth Jr., P.H. Sammon, Practical considerations for adaptive implicit methods in reservoir simulation, J. Comp. Phys. 62 (1985) 265.
[5] Ami Harten, High resolution schemes for hyperbolic conservation laws, J. Comput. Phys. 49 (1983) 357–393.
[6] F. Kwok, H.A. Tchelepi, Potential-based reduced newton algorithm for nonlinear multiphase flow in porous media, Journal of Computational Physics 227 (1) (1983) 706–727, doi:10.1016/j.jcp.2007.08.012.
[7] R.J. LeVeque, Numerical Methods for Conservation Laws, Birkhauser, Zurich, 1992.
[8] J. Ortega, W. Rheinboldt, Iterative Solution of Nonlinear Equations in Several Variables, Academic Press, New York, 1970.
[9] D.W. Peaceman, A nonlinear stability analysis for difference equations using semi-implicit mobility, Soc. Petrol. Eng. J. (1977) 79–91.
[10] G.W. Thomas, D.H. Thurnau, Reservoir simulation using an adaptive implicit method, SPE J. 23 (1983) 760.